Supplementary Material of "Note: Investigation of a Marx generator imitating a Tesla transformer"

B. H. McGuyer[1, a)]
Department of Physics, Columbia University, 538 West 120th Street, New York, NY 10027-5255, USA

(Dated: 1 July 2018)

CONTENTS

I. SUPPLEMENTARY MATERIAL

A. Spark discharges

Fig. 5 provides larger versions of the insets showing spark discharge in Figs. 1 and 3. These pictures and the supplemental video show that the Marx coil apparatus is able to re-breakdown previous discharge channels from past bursts, as is known to occur with Tesla transformers. This phenomenon is visible in photographs and videos because of convection during the time between bursts (about 8.3 ms here), similar to how convection produces a rising spark structure in a Jacob's ladder. In the photographs, it leads to comb-like discharge patterns, or the so-called "banjo effect," because bursts briefly illuminate each rising channel during the exposure. This process is similar to streak photography except that here the spark discharge is moving instead of the camera system. In the video, this is shown by the illusion of vertically rising discharge structures that evolve over time.

During testing of the Marx coil (MC) apparatus, the longest observed discharge lengths were roughly 15 cm for free discharge in air for operation with the solenoid as arranged in the inset of Fig. 3, and 20 cm for discharges from a wire to a flat grounded target without the solenoid as arranged in Fig. 4.

B. Marx-coil aparatus

The total height of the MC apparatus as shown in Fig. 1(a) was roughly 68 cm. The capacitors C_{1-17}, C_b, and C_t were Murata DHR series ceramic disc capacitors with a ZM temperature characteristic, ±10% tolerance, and 15 kV direct-current (DC) rating. Their capacitance is known to decrease with DC bias, up to roughly 22% at 15 kV.[1]

The inductors L_{1-36} were 3-pi universal wound Bourns/J. W. Miller 6306-RC varnished RF chokes with ferrite cores, ±5% tolerance, and 31 Ω or less DC resistance. These inductors were installed in one of two clear plastic tubes, each with a slot for the leads that was later sealed with room-temperature-vulcanizing (RTV) silicone, and the inductors were immersed in mineral oil.

The load inductor L_s was a close-wound single-layer solenoid made from a 55.4 cm varnished winding of approximately 791 turns of 22 awg magnet wire on a plastic pipe with an outer diameter of 8.8 cm. The measured inductance was 8.07 ± 0.03 mH at 10 kHz, and DC resistance was 11.8 ± 0.1 Ω. The estimated effective Medhurst self-capacitance[2] is ∼ 8 pF.

Note that coupling is expected between the load and stage inductors as installed. This coupling could be suppressed with different physical arrangements, or by using different winding patterns.[3] Alternatively, the load and stage inductors need not be separate components.

The solenoid base current was measured using a Pulse F15155NL current transformer with a 1 kΩ shunt resistor, which gave a sensitivity of 2 V/A over 0.5–700 kHz. The bandwidth limitations of the current transformer led to the initial measurement error in Fig. 3(b), and of a capacitive-pickup probe to the same (though less visible) in Fig. 4.

The spark gap electrodes were made of brass 4-40 acorn nuts with a radius of curvature of about 2.5 mm. The gap spacings used were roughly 3.0, 3.0, 3.0, 3.0, 3.0, 3.0, 3.5, 4.0, 4.5, 5.0, 5.5, 6.0, 6.5, 7.0, 7.5, 8.0, 8.0, and 8.0 mm, from bottom to top.

When installed, the plastic pipe form of the solenoid muffled and blocked the spark gap noise and light emission significantly. White plastic was used for the U-channel and solenoid pipe so that the interior space resembled an integrating cavity, in case it might reduce gap jitter and losses. Note that gap quenching is not critical here unlike in spark-gap Tesla transformers (SGTTs), since energy is not transferred between resonant circuits.

Two different toroidal output terminals were used for the data shown. The first, shown in Figs. 1 & 4, had a maximum width of 4.8 cm, height of 2.9 cm, and an estimated electrostatic capacitance of 5.5 pF. In Fig. 3, a second terminal was placed above the first terminal. This

[a)] Present address: Facebook, Inc., 1 Hacker Way, Menlo Park, CA 94025, USA

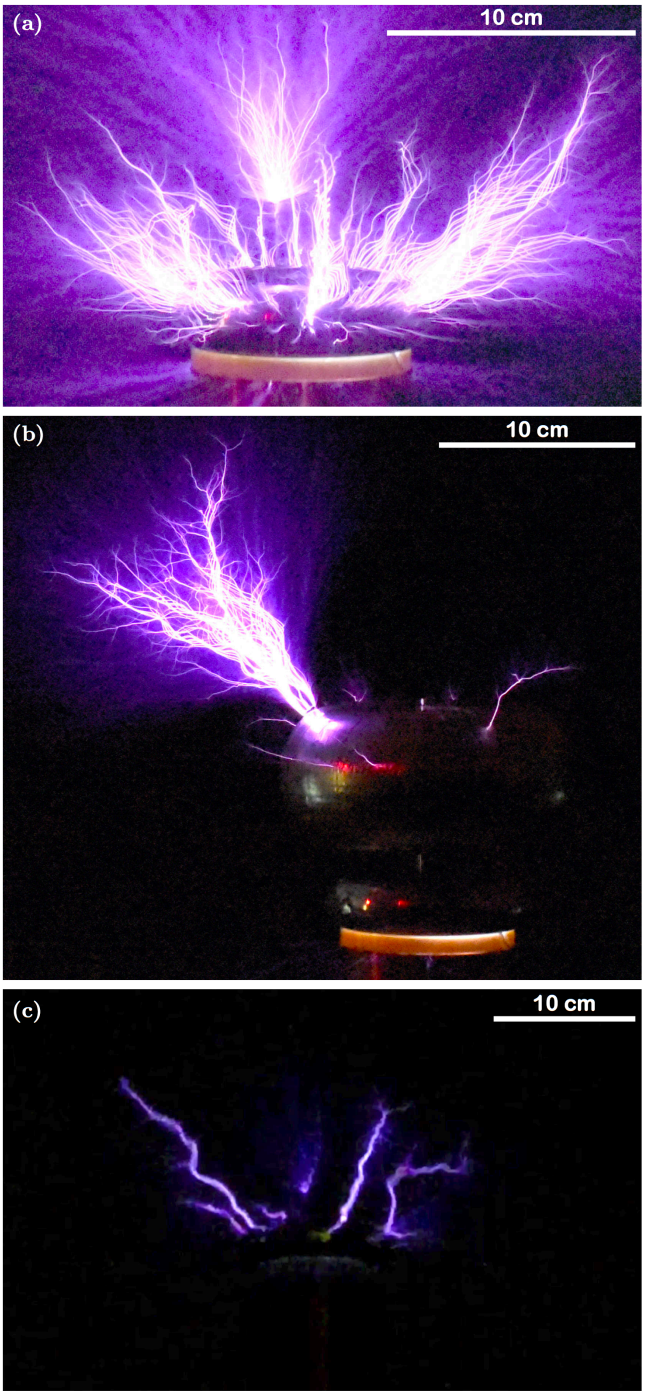

FIG. 5. Spark discharge photographs and video. (a) Larger version of inset in Fig. 1. A vertical, thin metal wire acted as a breakout point for several sparks that do not appear to connect to the output terminal. (b) Larger version of inset in Fig. 3, with a larger terminal placed above the terminal shown in (a). A piece of metal foil tape acted as a breakout point for the longest discharges. (c) Still image from supplementary video. The terminal arrangement is the same as in (a).

terminal had a maximum width of 15.3 cm, height of 7.0 cm, and an estimated electrostatic capacitance of 6.0 pF. A vertical metal wire segment was used as a breakout point for spark production in Figs. 1 and 4, and a folded piece of metal foil in Fig. 3.

A maximum value $C_{\max}$ for the charging capacitance can be roughly estimated from the power supply parameters and the repetition rate of 120 Hz as follows. Consider a 60 Hz AC power supply with rated output power $P = V_{\rm rms} I_{\rm rms}$ and output impedance $Z = V_{\rm rms}/I_{\rm rms}$, where $V_{\rm rms}$ and $I_{\rm rms}$ are the maximum root-mean-square output voltage and current. Then $C_{\max}$ corresponds to the capacitance that charges from zero voltage up to $\sqrt{2}\,V_{\rm rms}$ during a quarter cycle, or 1/240 second, at the rated power. From energy conservation this requires $C_{\max} V_{\rm rms}^2 = P/(240\ \text{Hz})$, which gives

$$C_{\max} = 1/(Z \times 240\ \text{Hz}). \tag{1}$$

For the NST of Fig. 2(e), $C_{\max} \approx 16.7$ nF. As built, the effective charging capacitance for the arrangement of Fig. 2(a) was 12.1 nF, and of Fig. 2(b) was about 11.8 nF, ignoring the NST filter capacitors (which added $\sim$ 0.24 nF).

In practice, the optimum charging capacitance that leads to the most energy per burst without significantly reducing the charging voltage should be found empirically, because NSTs are not ideal AC power supplies. Note that in practice charging may occasionally occur for longer (or shorter) than a quarter cycle, depending on the spark gap and load behavior, which can lead to larger charging voltages than the power supply rating.

The estimated erected Marx bank capacitance for the arrangement of Fig. 2(a) with the solenoid is 37 pF, and for that of Fig. 2(b) without the solenoid is 38.5 pF. In practice, the total erected capacitance will include additional capacitance from the terminal and solenoid, as estimated above (neglecting their interaction), and to the environment. Approximating the NST as a short during a burst, the erected Marx inductance for Fig. 2(a) is roughly 7.4 mH and for Fig. 2(b) without the solenoid is roughly 90 mH.

C. Estimating time-dependent circuit parameters

During operation, the apparatus behaves approximately like a damped, undriven RLC circuit with time-dependent parameters. This is because during a burst the spark gaps act approximately as short circuits, making the circuit in Fig. 2 resemble that of Fig. 6. The circuit parameters and their time dependence can be estimated from "variable RLC fits" to the data in the following manner.

Consider a lumped series RLC circuit as sketched in Fig. 6. Let us assume that the inductance L is constant, but that the resistance $R = R(t)$ and capacitance $C = C(t)$ may vary in time. This follows from noting that the inductance is set mainly by the inductors L_1 to L_{36} and L_s, which are not expected to vary during operation except when the solenoid L_s is removed, in which case

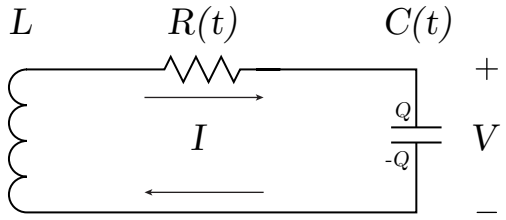

FIG. 6. Lumped series RLC circuit with constant inductance L and time-dependent resistance $R(t)$ and capacitance $C(t)$.

the increased current through the stage inductors may lead to saturation. Following Kirchoff's voltage law, the circuit satisfies the differential equation

$$(LI)' + RI + Q/C = 0. \tag{2}$$

Here and subsequently a prime denotes differentiation with respect to time t. Using this with $I = Q'$, the charge $Q(t)$ then evolves according to the differential equation

$$Q'' + \left(\frac{R}{L}\right) Q' + \left(\frac{1}{LC}\right) Q = 0, \tag{3}$$

which has the same form as that for an RLC circuit with constant parameters. The current and voltage, however, will not evolve according to this equation. Instead, multiplying (3) by LC and differentiating gives the corresponding equation for the current $I(t)$,

$$I'' + \left(\frac{R}{L} + \frac{C'}{C}\right) I' + \left(\frac{1 + RC' + R'C}{LC}\right) I = 0. \tag{4}$$

Similarly, the voltage $V(t)$ across the capacitance $C(t)$ evolves according to

$$V'' + \left(\frac{R}{L} + \frac{2C'}{C}\right) V' + \left(\frac{1 + RC' + LC''}{LC}\right) V = 0, \tag{5}$$

which follows from (3) using $Q = CV$ and assuming $C(t) \neq 0$.

To determine the circuit parameters from measurements of the current $I(t)$ or voltage $V(t)$, the differential equation was approximately reconstructed by fitting the data with the trial function

$$y(t) = A_0 e^{-B(t)} \cos[D(t) + \phi_0], \tag{6}$$

where the fit parameters A_0 and ϕ_0 are constant but the functions $B(t)$ and $D(t)$ depend on time. This form assumes the burst start time is known, and that there is no background offset (which was removed by fitting with an offset parameter). This trial function satisfies the differential equation

$$y'' + U(t)\, y' + W(t)\, y = 0 \tag{7}$$

where the functions $U(t)$ and $W(t)$ may be computed as

$$U(t) = 2B' - D''/D' \tag{8}$$

$$W(t) = (B')^2 + (D')^2 + B'' - B'D''/D'. \tag{9}$$

The data presented here was described well by the trial function (6) using the polynomials

$$B(t) = \alpha_1 t + \alpha_2 t^2 + \alpha_3 t^3 \tag{10}$$

$$D(t) = \omega_1 t + \omega_2 t^2 + \omega_3 t^3, \tag{11}$$

where the fit parameters α_i and ω_i are independent of time. In contrast, an RLC circuit with constant parameters is described by the polynomials $B(t) = t\,R/(2L)$ and $D(t) = t\sqrt{1/(LC)^2 - R^2/(2L)^2}$.

After fitting data with the trial function (6), the reconstructed differential equation (7) may be used with the appropriate differential equation from above to estimate the time-dependent circuit parameters $C(t)$ and $R(t)$. For the data presented here, this analysis was simplified using the following approximations. For the current data, the approximation

$$|RC' + R'C| \ll 1 \tag{12}$$

simplifies the differential equation (4) to

$$I'' + \left(\frac{R}{L} + \frac{C'}{C}\right) I' + \left(\frac{1}{LC}\right) I \approx 0. \tag{13}$$

Using this with (7), the circuit parameters may be estimated using L, (8–11), and the fit parameters α_i and ω_i as

$$C(t) \approx 1/[L\,W(t)] \tag{14}$$

$$R(t) \approx L\,[U(t) + W'(t)/W(t)] \tag{15}$$

within the fitted range of times while $I(t)$ may be distinguished from noise. Likewise, for the voltage data the approximation

$$|RC' + LC''| \ll 1 \tag{16}$$

simplifies the differential equation (5) to

$$V'' + \left(\frac{R}{L} + \frac{2C'}{C}\right) V' + \left(\frac{1}{LC}\right) V \approx 0. \tag{17}$$

In this case, the circuit parameters may be estimated as

$$C(t) \approx 1/[L\,W(t)] \tag{18}$$

$$R(t) \approx L\,[U(t) + 2W'(t)/W(t)]\,, \tag{19}$$

again, within the fitted range of times while $V(t)$ may be distinguished from noise. For both cases, after estimating $C(t)$ and $R(t)$ the initial approximation, either (12) or (16), must be tested for consistency.

D. Data analysis

Tables I and II list the fixed and variable RLC fit parameters for the fit curves shown in Figs. 3 and 4 of the paper and the additional fit curves in Fig. 7. The additional current data in Fig. 7 corresponds to nearly

TABLE I. Fixed RLC fit parameters for data in Figs. 3 and 7 using the form (20). The offset I_0 is excluded. Values in parenthesis are uncertainties in the last digits. The variation between parameters with and without discharge is comparable to that observed between data sets with the same conditions.

Data set	A_0 Amp	τ μs	$\omega/(2\pi)$ kHz	t_0 μs
MC with discharge	16.7(2)	15.1(2)	279.64(14)	−0.030(6)
MC without discharge	14.4(2)	13.5(2)	277.96(15)	−0.036(6)

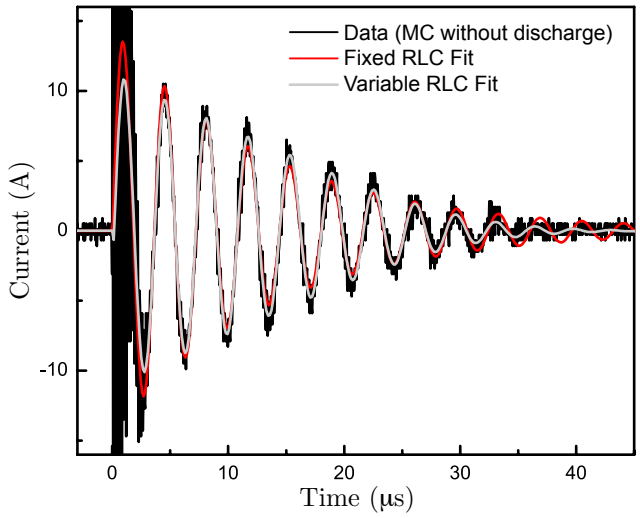

FIG. 7. Current data and fits corresponding to the "MC without discharge" curves of Figs. 9(a) and 10 and parameters of Tables I and II.

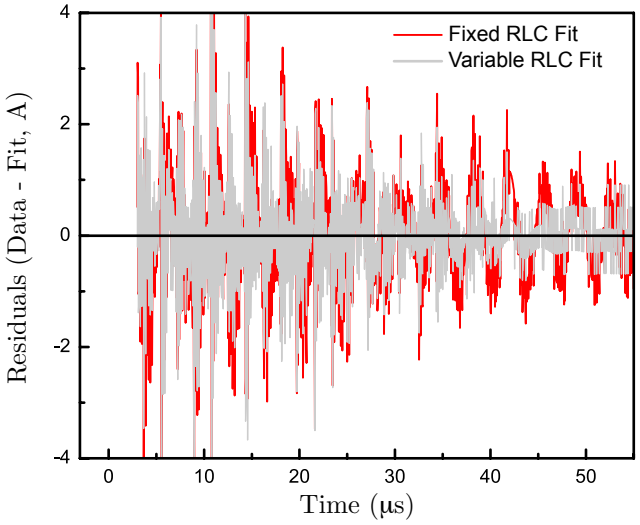

FIG. 8. Fit residuals for Fig. 3.

identical conditions as those in Fig. 3, except that the breakout point was removed to prevent any visible discharge. Fig. 8 shows residuals for the fits of Fig. 3, highlighting how the variable RLC fit is an improvement over the fixed RLC fit.

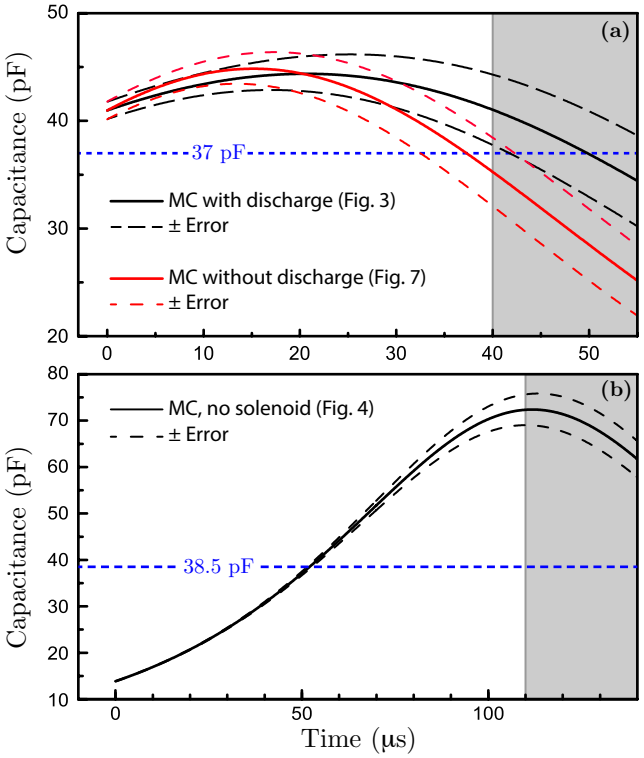

FIG. 9. Estimated capacitance from variable RLC fits of measured current or voltage waveforms. (a) MC operation with the solenoid. The black curve is from the data in Fig. 3(b), while the red curve is from data in Fig. 7 in similar conditions but without visible discharge (the breakout point was removed). (b) MC operation without the solenoid. The curve is from the data in Fig. 4 and is likely affected by inductor saturation effects that violate the assumption of constant inductance. Dashed curves show the error from least-squares fit-parameter uncertainties. Horizontal blue dashed lines are the estimated erected Marx bank capacitances, without solenoid and terminal contributions. Grey regions mark when the waveforms are comparable to noise, and the capacitances less reliable.

The fixed RLC fits were of the form

$$I(t) = \begin{cases} 0, & t < t_0 \\ I_0 + A_0\, e^{-(t-t_0)/\tau} \sin[\omega(t-t_0)], & t \geq t_0. \end{cases} \quad (20)$$

For all current and voltage data, the time axis origin was manually set to match the time of the first signal observed on the oscilloscope. Fitting of the current data in Fig. 3(b) and Fig. 7 excluded the first 3 μs of data because of current transformer bandwidth limitations. Likewise, fitting of the voltage data in Fig. 4 excluded the first 2μs because of capacitive-pickup probe limitations.

The variable RLC fits used a modified version of (6) described above that includes an offset,

$$y(t) = \begin{cases} 0, & t < t_0 \\ y_0 + A_0\, e^{-B(t-t_0)} \cos[D(t-t_0) + \phi_0]. & t \geq t_0, \end{cases} \quad (21)$$

TABLE II. Variable RLC fit parameters for data in Figs. 3, 4, and 7 using the form (21) with expansions (10) and (11). The offset y_0 is excluded. Values in parenthesis are uncertainties in the last digits. The variation between parameters with and without discharge is comparable to the variation observed between different data sets with the same conditions.

Data set	A_0 Amp	$\alpha_1 \times 10^3$ MHz	$\alpha_2 \times 10^4$ MHz^2	$\alpha_3 \times 10^6$ MHz^3	ω_1 rad MHz	$\omega_2 \times 10^3$ rad MHz^2	$\omega_3 \times 10^6$ rad MHz^3	ϕ_0 degree
MC with discharge	14.2(5)	58(9)	−18(6)	69(12)	1.815(8)	−3.4(6)	53(11)	−100(2)
MC without discharge	11.3(4)	42(9)	−4(7)	54(15)	1.815(9)	−5.3(7)	113(14)	−107(2)
MC, no solenoid	–	31.2(9)	−2.7(3)	2.6(2)	0.8946(9)	−4.45(2)	12.9(2)	175.6(4)

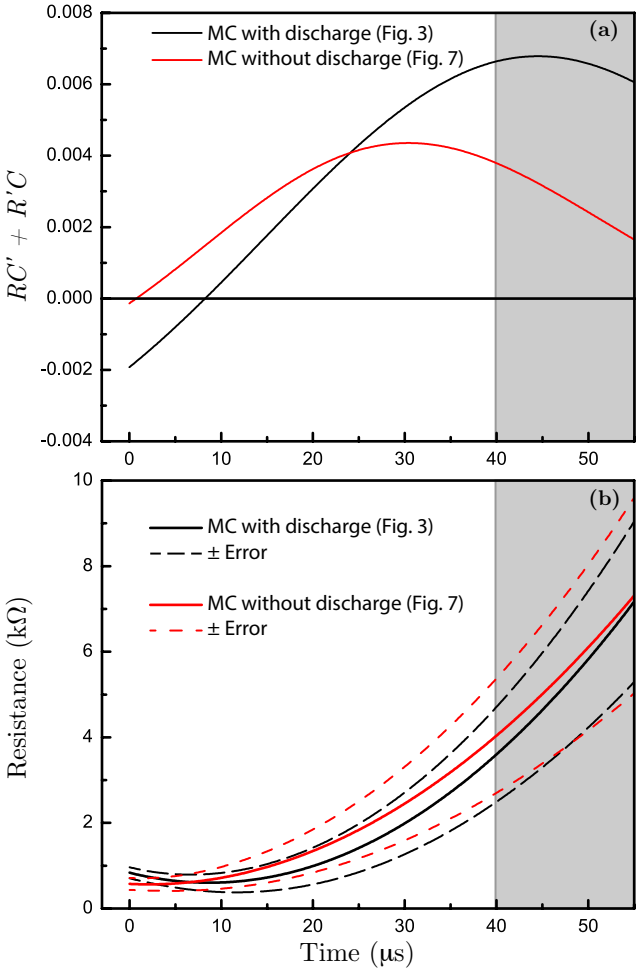

FIG. 10. Parameter estimation from variable RCL fits of the data in Figs. 3 and 7 using fit parameters in Table II. (a) Check of the approximation (12). (b) Estimate of resistance using (15) that corresponds to the capacitance of (14) shown in Fig. 9(a).

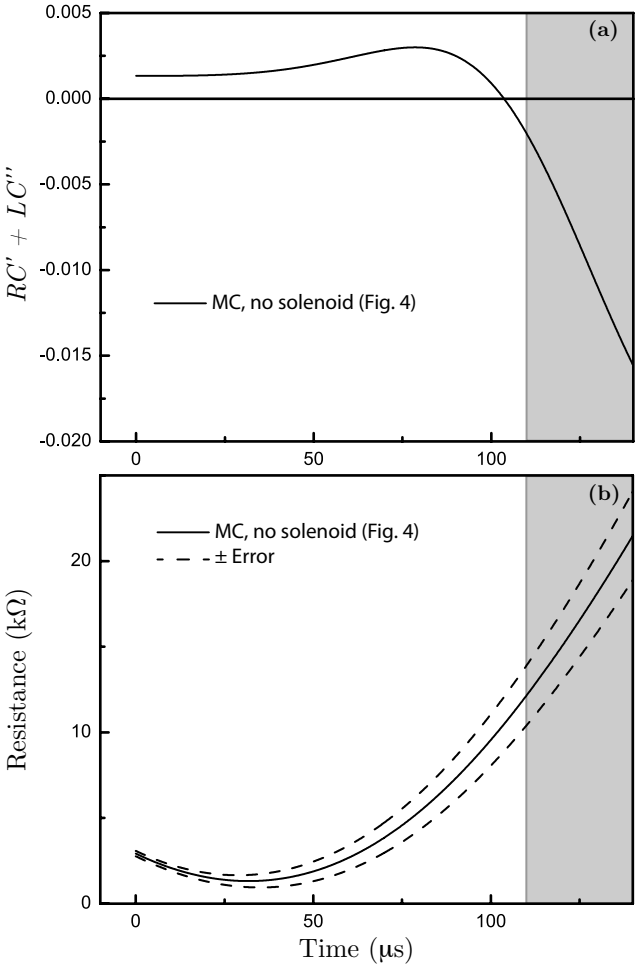

FIG. 11. Parameter estimation from the variable RCL fit of the data in Figs. 4 using fit parameters in Table II. (a) Check of the approximation (16). (b) Estimate of resistance using (19) that corresponds to the capacitance of (18) shown in Fig. 9(b).

As before, the time axis origin was manually set to match the time of the first signal observed on the oscilloscope. However, here t_0 was manually set to zero before fitting.

Fig. 9 shows reconstructed capacitances for the data of Figs. 3, 4, and 7 using the approach described in the previous section. This reconstruction assumes the effective inductance is constant, which is likely a good approximation for the data of Figs. 3 and 7. Unfortunately, no reproducible trend was observed in this and other data that could be attributed to spark discharge, likely because of a larger variability in component effects.

The solenoid was removed for the data of Fig. 4, increasing the current flowing through the stage inductors and potentially saturating their ferrite cores. Therefore, the reconstruction for the data of Fig. 4 is likely incorrect, and instead represents a fictitious set of time-varying RC

parameters with constant inductance that would lead to a similar voltage waveform.

The capacitance estimation of Fig. 9 used an inductance L of 7.4 mH for the current data with the solenoid and of 90 mH for the voltage data without the solenoid. Figs. 10 and 11 provide consistency checks of the approximations (12) and (16) required for this estimation, and show corresponding estimated resistances. The dashed curves shown in Figs. 9, 10, and 11 were estimated from error propagation of the fit parameter uncertainties.

For Fig. 3, the inferred maximum voltage using the variable RLC fit is 201 kV (using the fixed RLC fit, 228 kV). The charging voltage can be approximated as this divided by 18, giving 11.2 kV, which is close to the maximum value of 12.4 kV expected from the power supply in Fig. 2(e) with the Variac set to 140 $V_{\rm rms}$ assuming a 120 Hz repetition rate. For an erected bank capacitance of 37 pF, this corresponds to a charging energy of at least 0.75 J in the Marx bank. Including estimates for the solenoid and terminal contributions given above, the total effective output capacitance is roughly 50.5 pF, which corresponds to a charging energy of 1.0 J.

E. Discharge loading of Tesla transformers

Unfortunately, the effects of spark discharge loading on Tesla transformers have not been extensively studied.[4] Neither has the related subject of optimizing a Tesla transformer to generate the longest discharge over single or multiple pulses, unlike optimizing to produce the maximum voltage in a single pulse without discharge.[5] These two goals are not identical because nonuniform electric fields normally create the discharge and the longest discharges may form over multiple pulses.

However, the common approach to maximize the discharge length for a Tesla transformer provides suggestive evidence[6] for capacitive loading by spark discharge. This approach is described in Ref. 6 and in online resources for Tesla coil enthusiasts,[7] and consists of empirically lowering the uncoupled self-resonant frequency of the primary below that of the secondary until the longest discharge is obtained. This approach is often initiated by first attaching a wire to simulate the desired discharge, and then tuning the primary to be resonant with the perturbed secondary before further optimization.

Presumably, this approach of detuning the primary enables a Tesla transformer to tolerate a larger discharge load during operation.[8] However, this has not been extensively studied and it is possible that dynamical effects such as rapid adiabatic passage may contribute.[9] In contrast, the output voltage of a single pulse is maximized by adjusting the resonant frequencies and coupling strength to particular theoretical values.[5]

F. Further improvements

The Marx coil apparatus presented here was not optimized for a particular application. Improvement is possible using better components, in particular, more stable capacitors and lower-loss switches that allow more control (e.g., solid-state switches or triggered spark gaps). Additionally, the MC circuit could be modified to control the output waveform envelope, as is common with Marx generators,[10] perhaps to better match the slowly modulated ("beating") envelope typical of a SGTT.

Alternatively, another possible opportunity to imitate SGTTs while avoiding their circuit sensitivity may be to drive the solenoid base in series with solid-state switches and feedback, using techniques similar to those in modern Tesla transformer designs,[6,11,12] instead of driving a solenoid in parallel with a Marx generator as implemented here.

[1] Mutata Manufacturing Co., Ltd., "High Voltage Ceramic Capacitors DC10-40kV," Catalog No. C41E-2 (2016).

[2] T. H. Lee, *Planar Microwave Engineering* (Cambridge University Press, Cambridge, 2004).

[3] Y. G. Chen, R. Crumley, S. Lloyd, C. E. Baum, and D. I. Giri, IEEE Trans. on Electromagn. Compat. **30**, 345 (1988).

[4] R. Craven, in *IEE Colloquium on Pulsed Power '97 (Digest No: 1997/075)* (1997) pp. 38/1–38/3.

[5] M. Denicolai, Rev. Sci. Instrum. **73**, 3332 (2002).

[6] D. H. McCauley IV, *DRSSTC: Building the Modern Day Tesla Coil; Electrical and Mechanical Design* (Eastern Voltage Research, `www.easternvoltageresearch.com`, 2006).

[7] For example: `http://www.hvtesla.com/tuning.html`, or more quantitatively, `http://www.loneoceans.com/labs/drsstc1/` (Accessed January 2018).

[8] This is how online resources for Tesla coil enthusiasts usually justify the approach of tuning the primary self-resonant frequency below that of the secondary to maximize discharge length. These resources typically state that this approach accommodates a dynamically increasing capacitive load from discharge, often referred to as "streamer loading".

[9] L. Novotny, Am. J. Phys. **78**, 1199 (2010).

[10] M. S. Naidu and V. Kamaraju, *High Voltage Engineering*, 2nd ed. (McGraw-Hill, New York, 1995).

[11] D. H. McCauley IV, *DRSSTC: Building the Modern Day Tesla Coil; miniBrute Reference Design* (Eastern Voltage Research, `www.easternvoltageresearch.com`, 2007).

[12] G. Guangyan, "QCW DRSSTC 1," `http://www.loneoceans.com/labs/qcw/` (Accessed July 2018).